



**HAL**  
open science

## Measurement of the $B(E2, 0^+_{-1} \rightarrow 2^+_{-1})$ in the $N = 16$ nucleus $^{26}\text{Ne}$

J. Gibelin, D. Beaumel, T. Motobayashi, N. Aoi, H. Baba, Y. Blumenfeld, Zs. Dombradi, Z. Elekes, S. Fortier, N. Frascaria, et al.

► **To cite this version:**

J. Gibelin, D. Beaumel, T. Motobayashi, N. Aoi, H. Baba, et al.. Measurement of the  $B(E2, 0^+_{-1} \rightarrow 2^+_{-1})$  in the  $N = 16$  nucleus  $^{26}\text{Ne}$ . *Physical Review C*, 2007, 75, pp.057306. 10.1103/PhysRevC.75.057306 . in2p3-00140867

**HAL Id: in2p3-00140867**

**<https://hal.in2p3.fr/in2p3-00140867>**

Submitted on 10 Apr 2007

**HAL** is a multi-disciplinary open access archive for the deposit and dissemination of scientific research documents, whether they are published or not. The documents may come from teaching and research institutions in France or abroad, or from public or private research centers.

L'archive ouverte pluridisciplinaire **HAL**, est destinée au dépôt et à la diffusion de documents scientifiques de niveau recherche, publiés ou non, émanant des établissements d'enseignement et de recherche français ou étrangers, des laboratoires publics ou privés.

# Measurement of the $B(E2, 0_1^+ \rightarrow 2_1^+)$ in the $N = 16$ nucleus $^{26}\text{Ne}$

J. Gibelin,<sup>1,2,\*</sup> D. Beaumel,<sup>1</sup> T. Motobayashi,<sup>3</sup> N. Aoi,<sup>3</sup> H. Baba,<sup>3</sup> Y. Blumenfeld,<sup>1</sup>  
Zs. Dombrádi,<sup>4</sup> Z. Elekes,<sup>4</sup> S. Fortier,<sup>1</sup> N. Frascaria,<sup>1</sup> N. Fukuda,<sup>3</sup> T. Gomi,<sup>3</sup> K. Ishikawa,<sup>5</sup>  
Y. Kondo,<sup>5</sup> T. Kubo,<sup>3</sup> V. Lima,<sup>1</sup> T. Nakamura,<sup>5</sup> A. Saito,<sup>6</sup> Y. Satou,<sup>5</sup> E. Takeshita,<sup>2</sup>  
S. Takeuchi,<sup>3</sup> T. Teranishi,<sup>7</sup> Y. Togano,<sup>2</sup> A. M. Vinodkumar,<sup>5</sup> Y. Yanagisawa,<sup>3</sup> and K. Yoshida<sup>3</sup>

<sup>1</sup>*Institut de Physique Nucléaire, IN2P3-CNRS, F-91406 Orsay, France*

<sup>2</sup>*Department of Physics, Rikkyo University, 3-34-1 Nishi-Ikebukuro, Toshima, Tokyo 171-8501, Japan*

<sup>3</sup>*RIKEN (The Institute of Physical and Chemical Research), 2-1 Hirosawa, Wako, Saitama 351-0198, Japan*

<sup>4</sup>*Institute of Nuclear Research of the Hungarian Academy of Sciences, PO Box 51, H-4001 Debrecen, Hungary*

<sup>5</sup>*Department of Physics, Tokyo Institute of Technology, Tokyo 152-8551, Japan*

<sup>6</sup>*Center for Nuclear Study, University of Tokyo, RIKEN Campus, 2-1 Hirosawa, Wako, Saitama 351-0198, Japan*

<sup>7</sup>*Department of Physics, Kyushu University, 6-10-1 Hakozaki, Higashi, Fukuoka 812-8581, Japan.*

(Dated: February 14, 2007)

Differential cross section of the inelastic scattering of a 54 MeV/u  $^{26}\text{Ne}$  beam on a lead target has been measured by detecting the de-excitation  $\gamma$ -rays. Analysis of the first  $2^+$  state angular distribution of the inelastically scattered nuclei shows that the process cannot be considered as a pure Coulomb excitation, and nuclear contribution must be taken into account. The charge deformation deduced,  $\beta_2^C = 0.392 \pm 0.024$ , corresponds to a  $B(E2) = 141 \pm 18 \text{ e}^2\text{fm}^4$  in agreement with a  $N = 16$  sub-shell closure.

PACS numbers: 23.20.-g; 25.45.De; 25.70.De; 25.60.-t

## I. INTRODUCTION

Nuclei with a closed shell play a special role in nuclear physics. They can be recognized among others from the relatively high excitation energy of their first excited state, a low value of the quadrupole electromagnetic transition probability  $B(E2, 0_1^+ \rightarrow 2_1^+)$ , sudden change in the binding energy or the nuclear radius when crossing a shell closure. The sub-shell closure at  $N=16$  was already revealed from the analysis [1] of the 1985 nuclear mass evaluation [2]. Recently, the change of nuclear radii at  $N=16$  has also been observed [3]. Non-observation of bound excited states in  $^{24}\text{O}$  is an indication for its doubly magic character and confirms the  $N = 16$  sub-shell closure at the neutron drip-line [4]. On the other hand, the sub-shell closure at  $N = 14$  was found to persist in neutron-rich oxygen isotopes [4–7].

For the neon isotopes, the relatively high energy of the first  $2^+$  state in  $^{24,26}\text{Ne}$  and the relatively small values of their  $B(E2, 0_1^+ \rightarrow 2_1^+)$  transition probabilities [8] were considered as signatures of the survival of the  $N=14,16$  sub-shell closures at  $Z=10$ . Recently, the  $B(E2, 0_1^+ \rightarrow 2_1^+)$  transition probability has been remeasured with a high precision for  $^{28}\text{Ne}$  [9]. The observed value was much smaller than the previous one [8], and even smaller than the accepted value for  $^{24,26}\text{Ne}$ . As a consequence, the trend of the  $B(E2)$  values shows a permanent decrease as a function of the neutron number from  $^{20}\text{Ne}$  to  $^{28}\text{Ne}$ , thus the signs of the  $N=16$  sub-shell closure seem to disappear, which contradicts the conclu-

sion that was drawn from the systematic behavior of the energy of the  $2_1^+$  states.

As a byproduct of a search for low-lying dipole strength in  $^{26}\text{Ne}$  [10], we have remeasured the  $B(E2)$  value in  $^{26}\text{Ne}$ .

## II. EXPERIMENTAL DETAILS

The experiment was performed at the RIPS facility [11] in RIKEN. A secondary  $^{26}\text{Ne}$  beam was produced by fragmentation of a 95 MeV/nucleon  $^{40}\text{Ar}$  primary beam impinging on a 2-mm-thick  $^9\text{Be}$  target. A typical intensity of the primary beam was 60 pA. An aluminum wedge of  $3.3^\circ$  with a mean thickness of 700 mg/cm<sup>2</sup> was used to improve the isotopic purity of the secondary beam. The  $^{26}\text{Ne}$  beam was produced with an energy of 58 MeV/u and of 80% purity. The main contaminants were  $^{27}\text{Na}$  ( $\approx 5\%$ ) and  $^{29}\text{Mg}$  ( $\approx 15\%$ ). The average beam rate was  $10^4$  pps with a momentum spread of 2%.

The particle identification of the incident beam was carried out event-by-event using the magnetic-rigidity-time-of-flight (TOF) method. The TOF was determined by the time difference between the cyclotron radio frequency signal and a 0.2 mm-thick plastic scintillator placed at the first focal plane of the RIPS separator. The incident beams were unambiguously identified.

The incident beam profile was monitored by two parallel-plate avalanche counters [12] placed in a chamber at the next focal plane of the RIPS at a distance of 148 cm and 118 cm upstream of the secondary natural Pb target of 230 mg/cm<sup>2</sup> (alternatively with a 130 mg/cm<sup>2</sup>  $^{27}\text{Al}$  target). The beam spot size and the beam angular spread at the target position were extrapolated to be 19 mm and  $1.4^\circ$  (FWHM) in the horizontal direction and 22 mm and  $1.2^\circ$  (FWHM) in the vertical direction,

---

\*gibelin@ipno.in2p3.fr; present address: Lawrence Berkeley National Laboratory, CA 94720 Berkeley, USA

respectively. The beam line section under vacuum was terminated by a  $25\ \mu\text{m}$  kapton window 2 cm before the secondary target.

The identification of the scattered particles as well as the measurement of their energy and scattering angle were performed using 8 silicon telescopes placed 1.2 m downstream of the target. They were at air but inside an aluminum chamber to protect them from ambient light. The entrance window of the chamber was made of  $7\ \mu\text{m}$  aluminised Mylar to minimize interactions with the incoming charged particles. A telescope was composed of two layers of silicon strip detectors (SSD) and one layer of lithium drifted silicon (Si(Li)) crystal. The two first layers of SSD were arranged in a  $3 \times 3$  matrix, with the middle one removed to avoid silicon detectors being hit directly by the beam. Each SSD had a  $50 \times 50\ \text{mm}^2$  active area and an 0.5 mm thickness. They were divided into 10 strips of 5 mm each. The first layer measured the horizontal position of the outgoing heavy ions and the second layer measured the vertical one. The back sides of SSDs were used for energy loss ( $\Delta E$ ) measurement. The residual energy was measured by the 3-mm-thick Si(Li) detectors from the MUST array [13]. Due to a bigger active area of  $55 \times 55\ \text{mm}^2$ , their positions were chosen to minimize the dead zones and the 8 detectors were shared among two layers of 4 units each, having overlapping dead zones. All nuclei of interest stopped in the Si(Li) detectors, allowing a total energy measurement with a resolution better than 1%. The particle identification was unambiguously done using the  $\Delta E$ - $E$  technique. This set of 8 telescopes allowed a very good angular coverage between  $1^\circ$  and  $5^\circ$ . The geometrical acceptance was deduced from simulation, taking into account both beam spread and straggling.

In order to minimize reactions of the beam particles with air we inflated a helium bag between the target and the silicon detector. Its entrance and exit windows were made of  $16\ \mu\text{m}$  Mylar. The pressure of the He gas inside was kept around 1 atm.

Gamma-rays produced in the secondary target were detected using the DALI2 array surrounding the target. It consisted of 152 NaI(Tl) and had a resolution (FWHM) of  $\sim 9\%$  at 662 keV [14]. The energy and efficiency calibrations of the NaI(Tl) detectors were made by using standard  $^{22}\text{Na}$ ,  $^{60}\text{Co}$ ,  $^{137}\text{Cs}$  and Am-Be sources. The absolute efficiency and the line shape of the  $\gamma$ -peak was reproduced by simulation using the GEANT 3 code [15]. The angular information was used for Doppler correction for  $\gamma$ -ray emitted from fast moving nuclei ( $\beta = 0.3$ ). For 2 MeV  $\gamma$ -rays the obtained resolution is 145 keV (FWHM) with an efficiency of  $13\% \pm 1.3\%$ .

### III. EXPERIMENTAL RESULTS

#### A. $\gamma$ -decay of $^{26}\text{Ne}$

The Doppler corrected energy spectrum for  $\gamma$  multiplicity strictly equal to 1 measured in coincidence with  $^{26}\text{Ne}$  scattered particles identified in the silicon telescope is presented in Fig. 1. The spectrum obtained with an empty target frame has been subtracted from the spectra with lead target after normalization to the same number of incident particles. The  $^{26}\text{Ne}$   $\gamma$  ray from the decay of the  $2_1^+$  state measured here at  $2022 \pm 62\ \text{keV}$  is clearly visible in it.

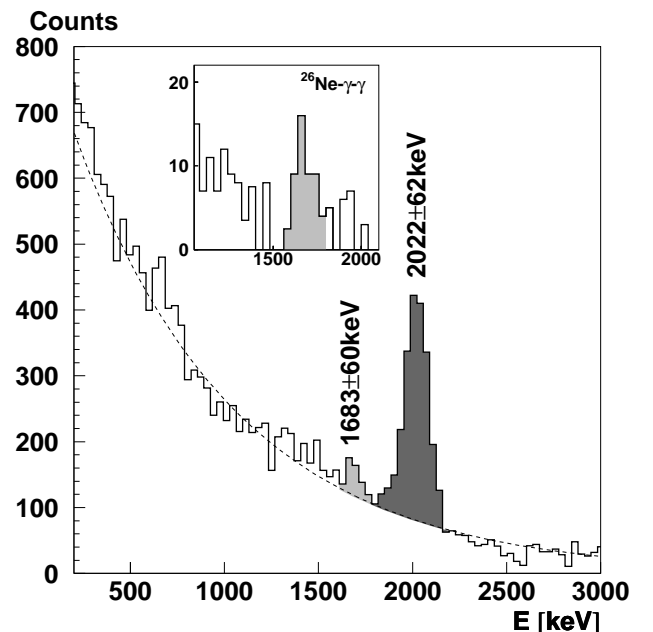


FIG. 1: Doppler corrected gamma energy distribution in coincidence with  $^{26}\text{Ne}$ . Inset:  $\gamma$ -ray energy spectrum, obtained with  $\gamma$ -multiplicity strictly equal to 2 and in coincidence with  $E(\gamma) = 2020\ \text{keV}$  transition.

In order to investigate the feeding of the  $2_1^+$  state through the decay of higher lying excited states, we examined the  $\gamma\gamma$  correlations. By gating on  $\gamma$ -ray energies between 1950 keV and 2090 keV, we observed a peak at  $1683 \pm 60\ \text{keV}$  (inset of Fig. 1) assigned to the cascade from the adopted 3691.2(3) keV state through the 2018.2(1) keV  $2_1^+$  state to the ground state. We estimated the ratio of the intensities of the 1667 keV/2018.2 keV lines to be  $10 \pm 5\%$ . In the following, this contribution to the 2 MeV  $\gamma$ -ray cross section will be taken into account.

### B. $B(E2)$ extraction using coupled channel equation code

To extract the  $B(E2)$  value from the  $2_1^+$  excitation cross section a distorted wave calculation was performed. Here we used the coupled channel equation code ECIS 97 [16] with optical potential parameters extracted from a  $^{20}\text{Ne}(40\text{MeV/n})+^{208}\text{Pb}$  reaction [17]. In the hypothesis that no nuclear interaction is involved (corresponding to a null nuclear deformation parameter  $\beta_2^N = 0.$ ) we deduced that a Coulomb deformation parameter  $\beta_2^C = 0.523 \pm 0.031$  reproduces our  $68 \pm 8$  mb cross section. This corresponds to a  $B(E2) = 250 \pm 30 \text{ e}^2\text{fm}^4$  in good agreement with the one of  $228(41) \text{ e}^2\text{fm}^4$  extracted with the same assumption (equivalent photon method) from the  $^{26}\text{Ne}(41.7\text{MeV/n})+\text{Au}$  inelastic scattering [8].

However, at these incident energies, a contribution from nuclear processes to the cross section may also be present. To check the validity of the assumption on pure Coulomb excitation we measured the angular distribution of inelastically scattered  $^{26}\text{Ne}$  in coincidence with the  $2020 \pm 150$  keV gamma-rays, presented in Fig. 2, where the background is removed by subtracting from the angular distribution gated by the 2020 keV peak the angular distribution gated on the adjacent area with the same  $\pm 150$  keV width. Note that the result is similar if we build the angular distribution from the number of 2 MeV counts (above background) for a given angle.

The experimental data are compared with the theoretical calculations convoluted by our detector response obtained using GEANT 3 simulations. The result is displayed in Fig. 2. The dashed line represents the case where pure Coulomb was assumed and the solid line is for the case with nuclear deformation included, with the hypothesis that its deformation length (i.e. the product  $\beta \cdot \text{radius}$ ) is equal to that of the electromagnetic one. Our resolution makes it difficult to deduce independently the nuclear and the Coulomb part of the excitation, but from Fig. 2, it can be seen that by taking into account the nuclear contribution the experimental data are better reproduced especially at small angles. The deduced deformation parameters are  $\beta_2^N = 0.403 \pm 0.025$  and  $\beta_2^C = 0.392 \pm 0.024$  which gives a  $B(E2) = 141 \pm 18 \text{ e}^2\text{fm}^4$ . Note that the  $\beta_2^N = \beta_2^C$  hypothesis gives a similar result.

In order to test our choice of optical potential we extracted the same quantities using parameters from the reaction  $^{40}\text{Ar}(41\text{MeV/n})+^{208}\text{Pb}$ [18]. For both the pure Coulomb case and that calculated by including the nuclear excitation we deduced a  $B(E2)$  only  $\sim 8\%$  greater than with the previous  $^{20}\text{Ne}$  potential. These values are therefore perfectly compatible – similarly to the study on  $^{28}\text{Ne}$  [9] – and by checking also that the corresponding angular distribution reproduces our data we conclude that the  $^{20}\text{Ne}+^{208}\text{Pb}$  optical potential is a reasonable choice.

In the following we compare our extracted value of  $141 \pm 18 \text{ e}^2\text{fm}^4$  with the experimental systematics of  $2_1^+$  energies and reduced transition probabilities both presented in Fig. 3. The open diamonds are the excitation

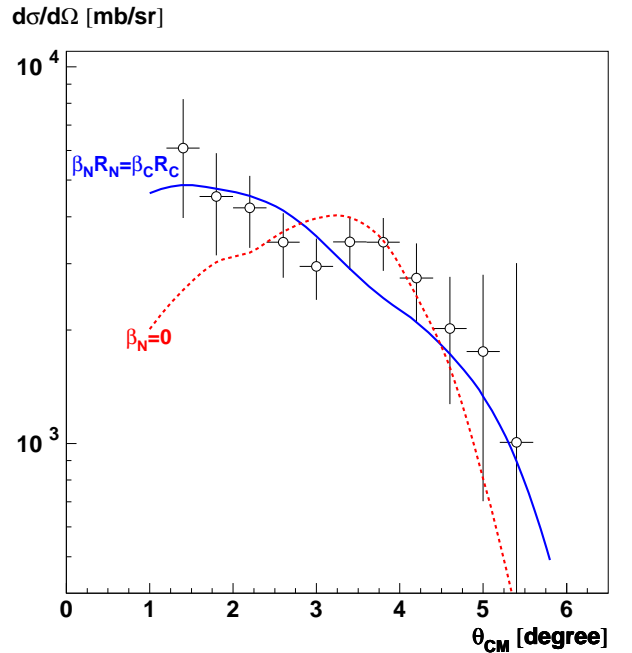


FIG. 2: The angular distribution for the first  $2_1^+$  excited state of  $^{26}\text{Ne}$  on a lead target is compared to an ECIS 97 calculation, convoluted by the detector response. We used the  $^{20}\text{Ne}(40\text{MeV/n})+^{208}\text{Ne}$  optical potential parameters. The solid line represents the case where a nuclear contribution is added,  $\beta_2^N = 0.403, \beta_2^C = 0.392$  whereas the dashed line represents the pure Coulomb case with  $\beta_2^N = 0, \beta_2^C = 0.523$ .  $R_{N,C}$  are the nuclear and the Coulomb radii respectively.

energies and the open circles are the previously accepted  $B(E2)$  values. Our result for the  $^{26}\text{Ne}$   $B(E2)$  and the recent extracted value for the  $^{28}\text{Ne}$  [9] are plotted with closed circle and closed triangle respectively. These last two analysis took into account the nuclear induced excitation and hence gave lower values than those measured previously, thus changing the overall trend. Before, the transition probability had a minimum for  $A = 24$  and presented a constant increase with neutron richness, hardly compatible with the  $N = 16$  sub-shell closure. Now the tendencies show a low plateau from  $A = 24$  to  $A = 28$  while the excitation energy is maximum for  $^{26}\text{Ne}$ . This combination is hence in agreement with the already accepted  $N = 16$  sub-shell closure.

### C. Nature of the 3.7 MeV excited state

In addition to the  $2_1^+$  state, another excited state at 3691 keV was populated in  $^{26}\text{Ne}$ . Earlier, a  $0^+$  spin-parity was assigned to a state at 3750 keV observed in the pion charge exchange reaction [19]. This spin assignment was retained to the 3691 keV in the  $\beta$ -decay study of  $^{26}\text{F}$  [20], although the presumably  $1^+$  ground state of  $^{26}\text{F}$  can decay to a  $2^+$  state, too, with the same probability. Here a  $0^+(\text{gs}) \rightarrow 0^+$  excitation is hardly compatible with our

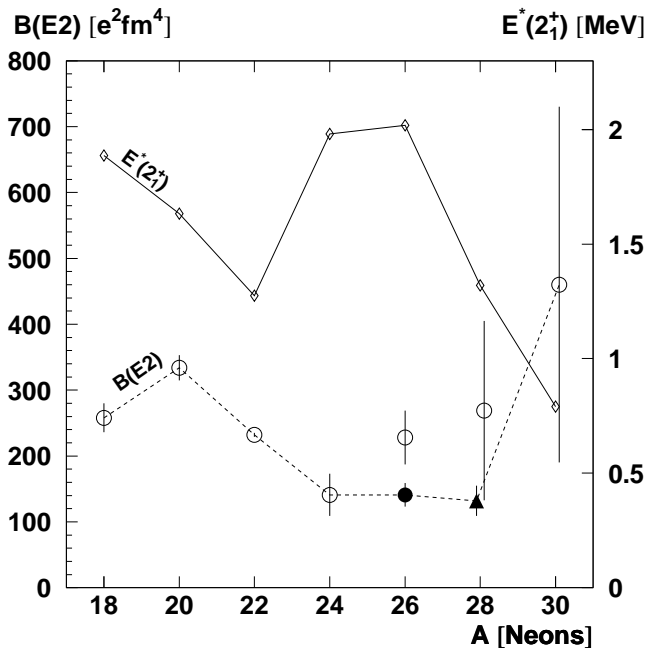


FIG. 3: Experimental  $2_1^+$  energy and  $B(E2; 0_1^+ \rightarrow 2_1^+)$  value for even neon isotopes. Open diamonds and open circles are previous experimental results for energy and transition probability respectively whereas the closed circle and the closed triangle are recent results. Lines (dashed and solid) are here to guide the eye only.

observed amount of  $7.2 \pm 4.2$  mb of  $\gamma$  production cross section for the 3.7 MeV state – forbidden by Coulomb excitation.

This is especially true for the inelastic scattering on an Al target measured in the same experiment, where a 3 times larger cross section was observed. One might assume that the ground state and the second  $0^+$  state are strongly mixed in  $^{26}\text{Ne}$ . However, this assumption clearly contradicts the shell model calculations. As an-

other possibility to explain the large excitation cross sections, we can consider giving up the  $0^+$  spin assignment to this state. The excitation of the  $2_2^+$  state has the next largest cross section in the coupled channel calculations (7 mb) in good agreement with the observation. From the present experiment this spin assignment seems to be a more reliable one. We mention that both the Monte Carlo shell model calculations [21] and the recent USD05 ( $a$  and  $b$ ) interactions [22] push the second  $0_2^+$  state to much higher energies (4.5, 4.7 and 5.7 MeV respectively) than the present value of 3.7 MeV whereas their  $2_2^+$  is located at 3.4, 3.7 and 3.8 MeV respectively, in good agreement with the experiments.

#### IV. CONCLUSION

Summarizing our results, we have measured the differential cross section of inelastic scattering of an intermediate energy radioactive  $^{26}\text{Ne}$  beam on a Pb target. From the coupled channel analysis of the inelastically scattered Ne nuclei we deduced the reduced transition probability for exciting the first  $2_1^+$  state to be  $B(E2) = 141 \pm 18 e^2\text{fm}^4$ , in agreement with a  $N = 16$  sub-shell closure. We also propose assigning a  $2^+$  spin-parity value to the 3.7 MeV second excited state.

#### Acknowledgments

We wish to acknowledge the useful discussions and help on ECIS 97 of N. Alamanos, A Gillibert and S. Shimoura. We would like to thank the RIKEN cyclotron operations and facilities staff for their help in performing the experiment. Financial support for the Franco/Japanese collaboration was provided by the French Ministry of Foreign Office *via* a Lavoisier scholarship and the university agreement of the College-Doctoral Franco-Japonais. This work has also financially been supported by the OTKA (Hungarian Research Fund) under contract Nos. F60438, T42733 and T46901.

- 
- [1] A. Abzouzi, M. Antony, and V. Ndocko Ndongue, *Il Nuovo Cimento A* **97**, 753 (1987).
  - [2] A. H. Wapstra and G. Audi, *Nucl. Phys. A* **432**, 1 (1985).
  - [3] A. Ozawa et al., *Phys. Rev. Lett.* **84**, 5493 (2000).
  - [4] M. Stanoiu et al., *Phys. Rev. C* **69**, 034312 (2004), .
  - [5] P. G. Thirolf et al., *Phys. Lett. B* **485**, 16 (2000).
  - [6] E. Becheva et al., *Phys. Rev. Lett.* **96**, 012501 (2006).
  - [7] Z. Elekes et al., *Phys. Rev. C* **74**, 017306 (2006), .
  - [8] B. V. Pritychenko et al., *Phys. Lett. B* **461**, 322 (1999).
  - [9] H. Iwasaki et al., *Phys. Lett. B* **620**, 118 (2005), .
  - [10] J. Gibelin et al., *AIP Conference Proceedings* **802**, 198 (2005).
  - [11] T. Kubo et al., *Nucl. Ins. and Meth. B* **70**, 309 (1992), .
  - [12] H. Kumagai et al., *Nucl. Ins. and Meth. A* **470**, 562 (2001), .
  - [13] Y. Blumenfeld et al., *Nucl. Ins. and Meth. A* **421**, 471 (1999), .
  - [14] S. Takeuchi et al., *RIKEN Accel. Prog. Rep.* **36**, 148 (2002).
  - [15] R. Brun et al., *CERN DD/EE/84-1* (1986).
  - [16] J. Raynal, Unpublished (1997).
  - [17] T. Suomijarvi et al., *Nucl. Phys. A* **491**, 314 (1989), .
  - [18] T. Suomijarvi et al., *Nucl. Phys. A* **509**, 369 (1990), .
  - [19] H. Nann et al., *Phys. Lett. B* **96**, 261 (1980), .
  - [20] A. T. Reed et al., *Phys. Rev. C* **60**, 024311 (1999).
  - [21] M. Belleguic et al., *Phys. Rev. C* **72**, 054316 (2005), .
  - [22] B. A. Brown and W. A. Richter, *Phys. Rev. C* **74**, 034315 (2006), .